Supplementary Information

Modulating Ligand-to-Metal Charge Transfer in Titanium-Oxo Clusters Enables Efficient H_2O_2 Activation and Pollutant Degradation

Zihang Wang[a]‡, Wenxin Peng[a]‡, Jintao Geng[a], Hui Wang[a]*, Xiaodong Zhang[a]*, and Yi Xie[b]

[a] Hefei National Research Center for Physical Sciences at the Microscale, University of Science and Technology of China, Hefei, 230026, P. R. China.

[b] State Key Laboratory of Precision and Intelligent Chemistry, University of Science and Technology of China, Hefei, Anhui 230026, China.

Experimental section:

Synthesis of Ti-PA.

Ti-PA was synthesized by a one-step solvothermal method.[1] In detail, propionic acid (5.5 mL), formic acid (0.06 mL) were mixed at room temperature; then dropwise $Ti(O^iPr)_4$ (0.92 mL, 3.0 mmol) was added. The resultant solution was heated at 80°C for four days. After cooled to room temperature, colorless crystals of Ti-PA were obtained, washed with excess amount of isopropanol and dried in air.

Synthesis of Ti-INA.

Ti-INA was synthesized by a one-step solvothermal method.[2] In detail, phenylphosphonic acid (0.104 g, 0.66 mmol), isonicotinic acid (0.172g, 1.3 mmol), and isopropyl alcohol (5.5 mL) were mixed at room temperature; then dropwise $Ti(O^iPr)_4$ (0.92 mL, 3.0 mmol) was added. The resultant solution was heated at 80°C for four days. After cooled to room temperature, colorless crystals of Ti-INA were obtained, washed with excess amount of isopropanol and dried in air.

Synthesis of other titanium-oxo clusters.

Ti_{32}[3], PTC-49[4], PTC-50[5], PTC-51[5], PTC-162[1], PTC-166[1], PTC-1[2], PTC-2[2], PTC-7[2], PTC-10[2], PTC-13[2], PTC-156[1], PTC-157[1], Ti_8Cat_2[6] and PTC-195[7] were synthesized according to previous reports.

Experiments for photo-Fenton-like degradation of pollutants.

5 mg of catalyst was dispersed into a 60 mL quartz tube containing 50 mL pollutants aqueous solution (10 mg/L). Then, it was stirred at 800 rpm to reach the adsorption-desorption equilibrium between the solution and sample in the absence of light. After 30 min, 4mM H_2O_2 was added into the reaction system, in the meantime, the quartz bottle was irradiated with visible light (420 nm$\leq \lambda \leq$780 nm) of a xenon lamp (CEL-HXF300, Beijing China Education Au-light Technology Co., Ltd.) at room temperature. With continuous stirring, the absorbance of 3 mL solution was measured by UV-vis spectrophotometer at an interval of 60 min. The calculation formula for photocatalytic efficiency is as follows: Photocatalytic effciency = $(C_0 - C_t)/C_0 \times 100\%$, C_0: the initial absorbance, C_t: the absorbance at specific time.

Experiments for Fenton-like degradation of pollutants.

5 mg of catalyst was dispersed into a 60 mL quartz tube containing 50 mL pollutants aqueous solution (10 mg/L). Then, it was stirred at 800 rpm to reach the adsorption-desorption equilibrium between the solution and sample. After 30 min, a certain amount of H_2O_2 (30%) was added into the reaction system. With continuous stirring, the absorbance of 3 mL solution was measured by UV-vis spectrophotometer at an interval of 60 min. The calculation formula for degradation efficiency is as follows: degradation efficiency = $(C_0 - C_t)/C_0 \times 100\%$, C_0: the initial absorbance, C_t: the absorbance at specific time. To figure out the dominant active oxygen species, we performed scavenging experiments as the above-mentioned procedure with different amounts of scavengers (mannitol, 10mg; SOD, 20000 units/mg, 10 mg).

Experiments for TMB oxidation.

15 mg of 3,3',5,5'-tetramethylbenzidine (TMB) and 5 mg of catalyst were dispersed into 50 mL of HAc/NaAc buffer solution. Then, it was stirred at 800 rpm to reach the adsorption-desorption equilibrium between the solution and sample. After 30 min, 50 μL of H_2O_2 (30%) was added into the reaction system. By monitoring the absorbance around 370 nm, the oxidation degree of TMB was tested every 2 minutes with the aid of UV-vis spectrophotometer.

Electrochemical measurements.

All of the electrochemical measurements were performed in a three-electrode system on an electrochemical workstation (CHI760E, Chenhua Instruments Co., China) in 0.5 M Na_2SO_4 solution. In detail, a cleaned indium in oxide (ITO) substrate coated with the sample film served as the working electrode, a platinum (Pt) wire acted as the counter electrode and a standard Ag/AgCl electrode was used as the reference electrode. The sample electrode, with an area of approximately 1 cm^2, was prepared by depositing 100 μL of an aqueous slurry consisting of 10 mg of the prepared samples, 800 μL of ethanol, 200 μL of water and 100 μL of Nafion onto a cleaned indium tin oxide (ITO) glass substrate. For the current-time i-t curves, the bias-voltage was set to 0 V and 200 mM H_2O_2 (30%) was added. For the CV measurements, the samples were tested with a voltage range from -0.6 V to 1.2 V and 200 mM H_2O_2 (30%).

Characterizations.

The powder X-ray diffraction patterns were collected on a Philips X'Pert Pro Super diffractometer with Cu Kα radiation (λ=1.54178 Å). The energy-dispersive spectroscopy mapping analyses were recorded on a JEM-2100F field-emission electron microscope at an acceleration voltage of 200 kV. X-ray photoelectron spectroscopy (XPS) was acquired on an ESCALAB MKII with Mg Kα excitation source, regarding C 1s (284.8 eV) as the reference. Fourier transform infrared (FT-IR) spectra were collected on a Magna-IR750 FT-IR spectrometer in a KBr pellet, scanning from 4000 to 400 cm^{-1} at room temperature. The UV-vis absorption spectra were obtained on a PerkinElmer Lambda 950 UV-vis-NIR spectrophotometer. The ESR spectra were collected using a JEOL JES-FA200 electron spin resonance spectrometer.

Electron spin resonance trapping measurements.

After sonicating 30 seconds, 50 μL of the DMSO suspension of the sample (1 g L^{-1}) and 50 μL of H_2O_2 (30%) was injected into 500 μL of 5-tert-butoxycarbonyl-5-methyl-1-pyrroline N-oxide (BMPO) solution (50 mM). The mixed solution was examined by using a Bruker EMX plus model spectrometer operating at the X-band frequency (9.4 GHz) at ambient temperature.

In-Situ DRIFTS measurements

In situ diffuse reflectance infrared Fourier-transform spectroscopy (DRIFTS) measurements were performed by employing a Bruker IFS 66v Fourier-transform spectrometer equipped with a Harrick diffuse reflectance accessory at the Infrared Spectroscopy and Microspectroscopy Endstation (BL01B)

in NSRL in Hefei, China. The samples were held in a custom-fabricated IR reaction chamber which was specifically designed to examine highly scattering powder samples in the diffuse reflection mode. The chamber was sealed with two ZnSe windows. During the in situ characterization, 0.1 MPa of Ar was introduced into the chamber and the peaks of pristine catalyst was set as a reference. Each spectrum was recorded by averaging 256 scans at a 4 cm^{-1} spectral resolution.

DFT calculation details.

All the first principle DFT calculations are performed by Vienna Ab initio Simulation Package (VASP)[8]. The interaction between ionic cores and valence electrons was treated using the projector augmented-wave (PAW) method.[9] The exchange-functional was described by the generalized gradient approximation (GGA) of Perdew-Burke-Ernzerhof (PBE) functional.[10] The valence electronic states were expanded in a plane-wave basis set with a kinetic energy cutoff of 400 eV (ENCUT). The self-consistent calculations apply a convergence energy threshold of 10^{-5} eV and the force on each atom less than 0.02 eV/Å was set for convergence criterion of geometry relaxation. To simulate the isolated PTC molecule and eliminate spurious interactions between periodically repeated images, the molecule was placed at the center of a large cubic supercell with side lengths of 45 Å. The Brillouin-zone integration was sampled with single Γ point($1\times1\times1$). The DFT-D3 method was employed to consider the van der Waals interaction.[11]

The reaction energy ΔE was calculated according to the following equation:

$$\Delta E = E_{total} - (E_{PTC} + 2E_{H_2O_2})$$

where E_{total}, E_{PTC}, and $E_{H_2O_2}$ represent the total energies of the reaction product complex, the isolated PTC cluster, and the H_2O_2 molecule, respectively.

Supplementary figures and tables

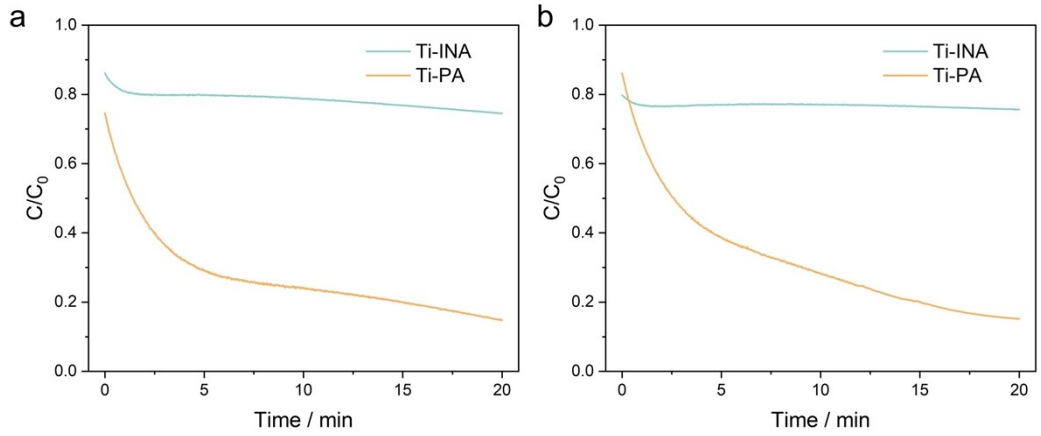

Figure S1. (a) and (b) Parallel experiments of MB-degradation kinetic curves by Ti-INA and Ti-PA.

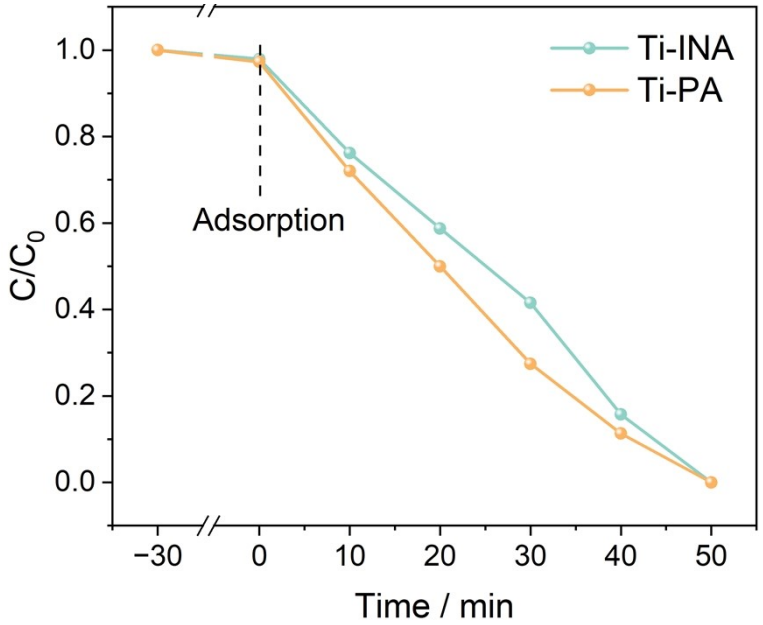

Figure S2. Photo-Fenton-like MB degradation by Ti-INA and Ti-PA.

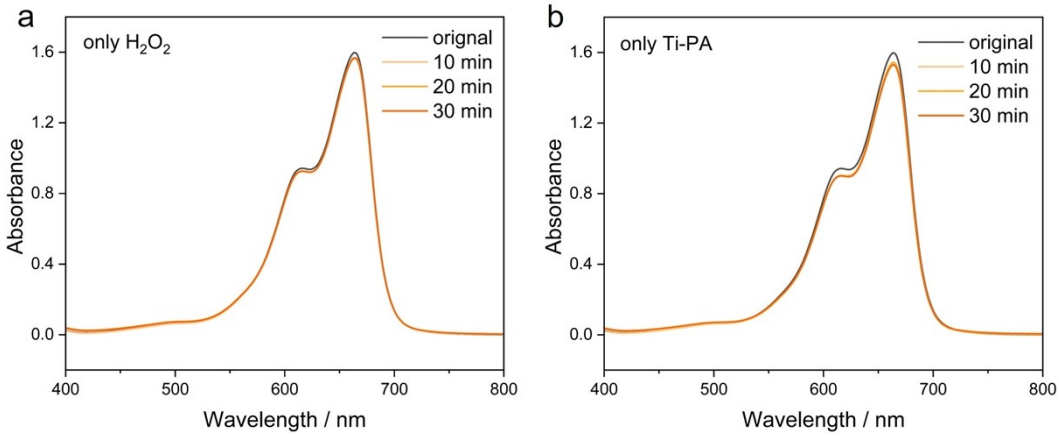

Figure S3. Time-dependent UV-vis absorption spectra of methylene blue (MB) degradation in the presence of bare H_2O_2 or Ti-PA.

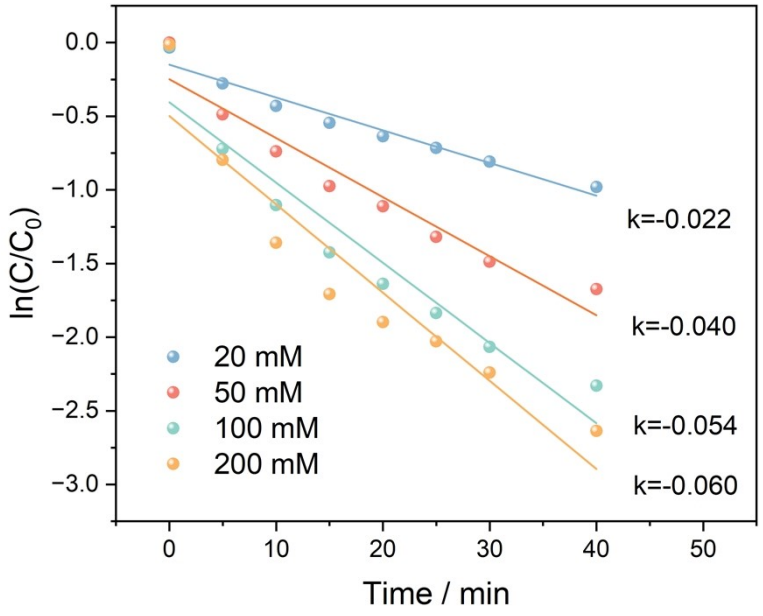

Figure S4. Rate constants of Fenton-like degradation at different concentrations.

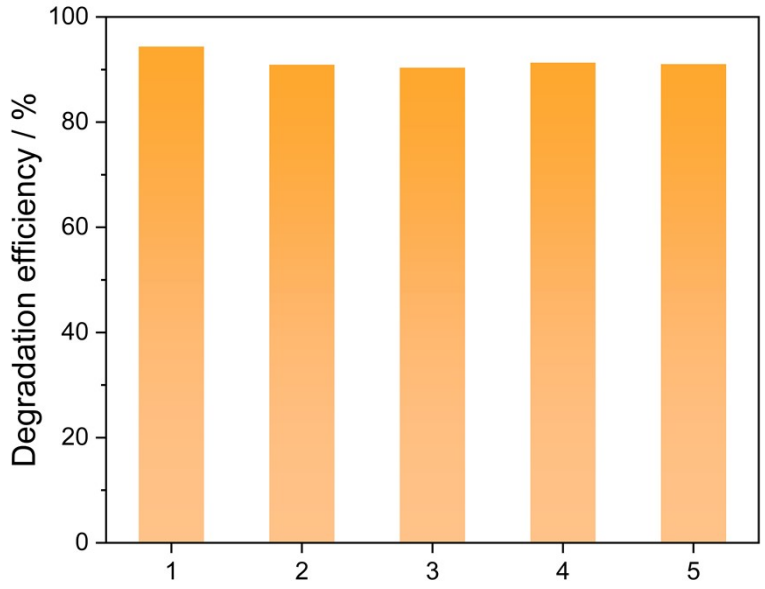

Figure S5. Cyclic MB degradation experiments by Ti-PA/H_2O_2.

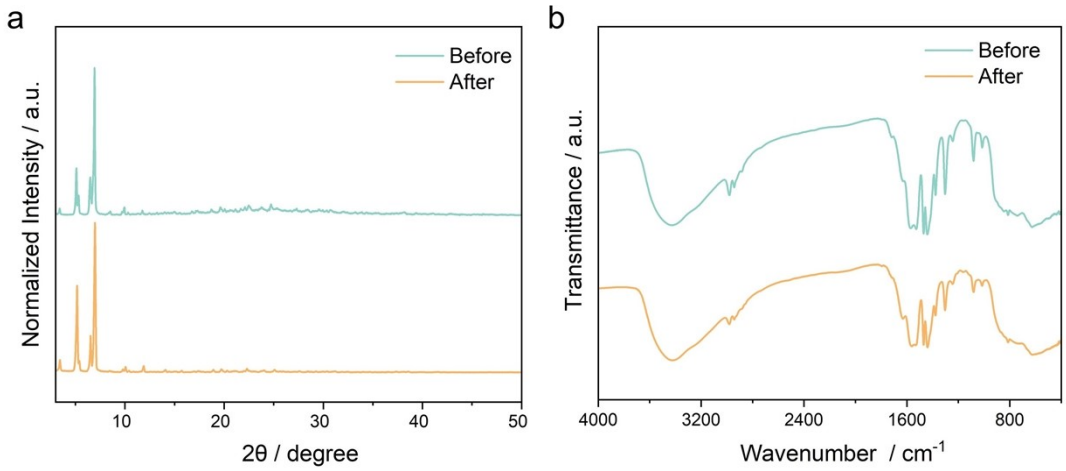

Figure S6. (a) XRD patterns and (b) FT-IR spectra of Ti-PA before and after the reaction.

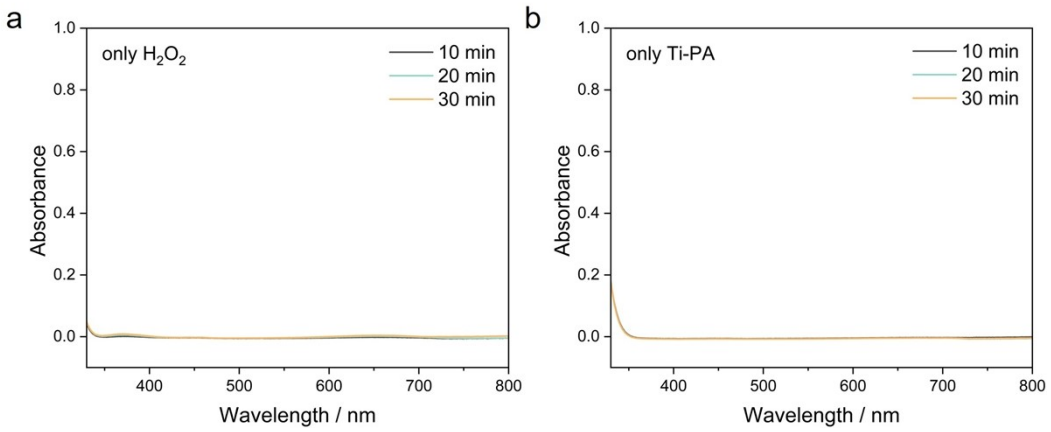

Figure S7. Time-dependent UV-vis absorption spectra of TMB oxidation in the presence of bare H_2O_2 or Ti-PA.

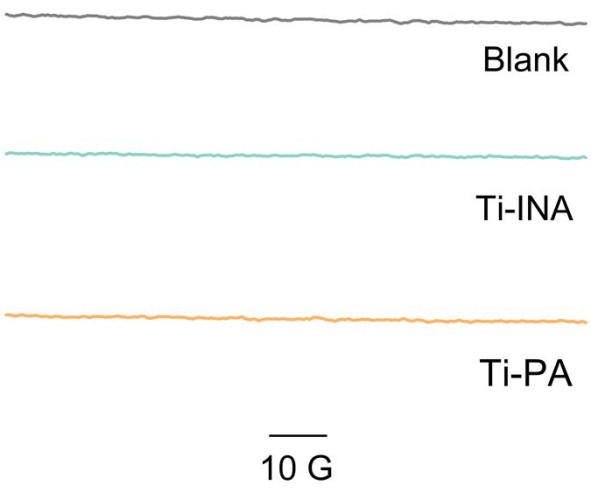

Figure S8. BMPO spin trapping ESR spectra for $\bullet O_2^-$ detection.

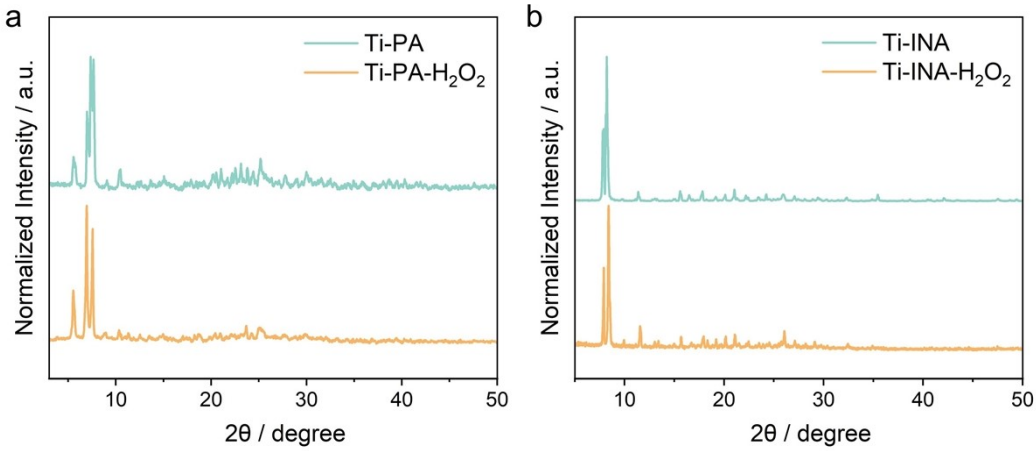

Figure S9. XRD patterns of (a) Ti-PA and Ti-PA-H_2O_2 and (b) Ti-INA and Ti-INA-H_2O_2

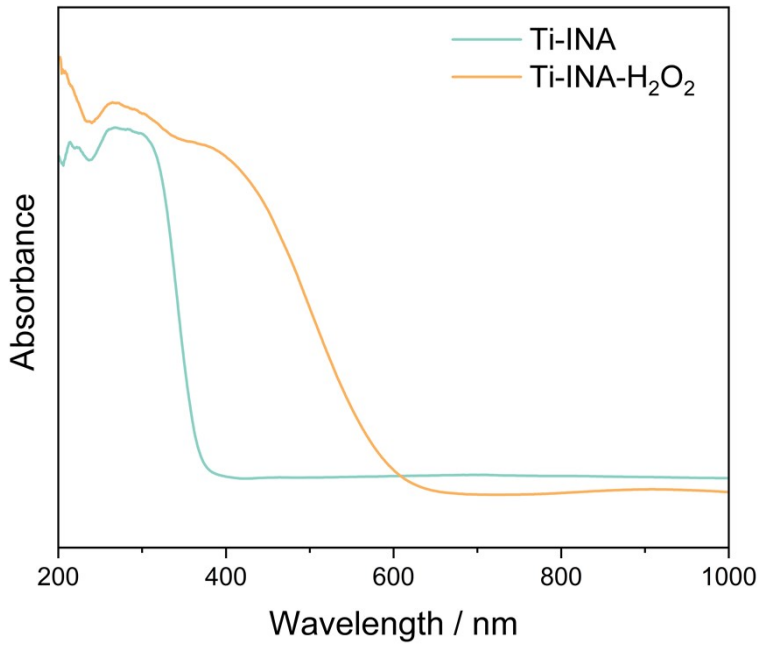

Figure S10. UV-vis absorption spectra of Ti-INA and Ti-INA-H_2O_2.

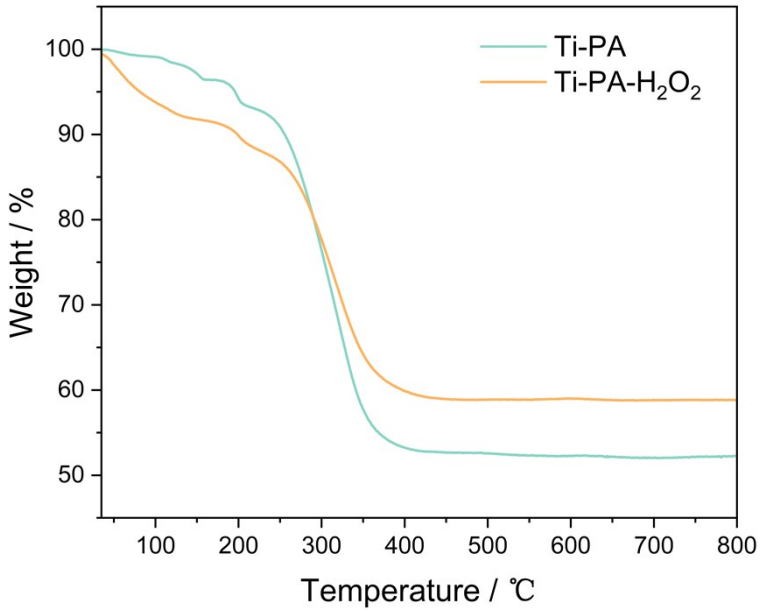

Figure S11. TG curves of Ti-PA and Ti-PA-H_2O_2.

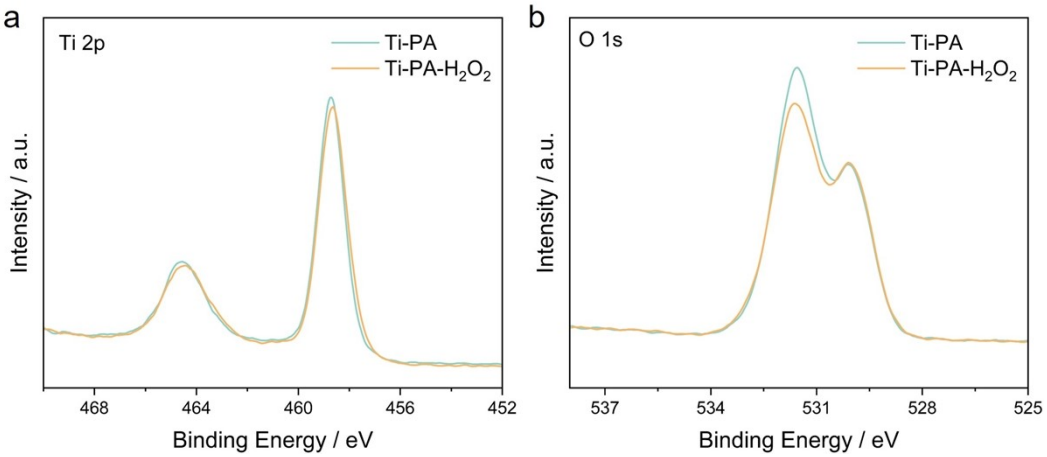

Figure S12. High-resolution (a) Ti 2p and (b) O 1s XPS spectra of Ti-PA and Ti-PA-H_2O_2.

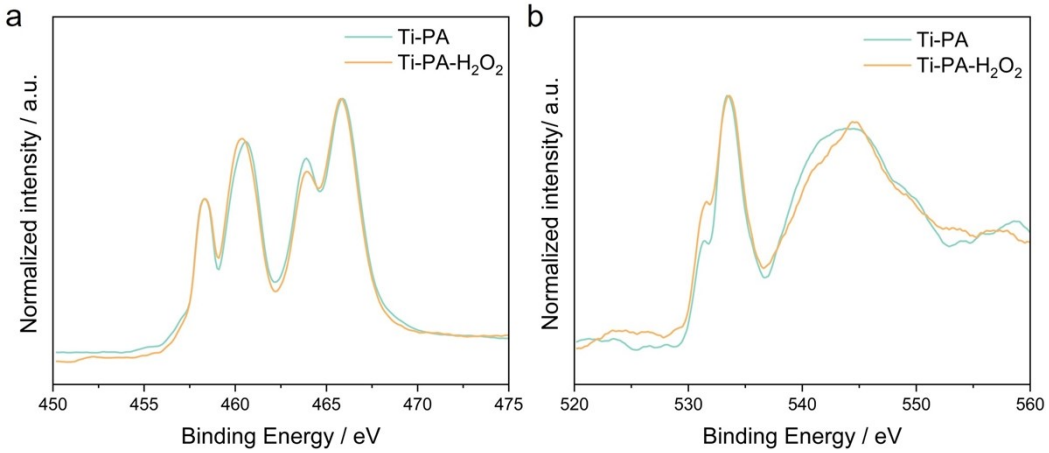

Figure S13. Normalized Ti L-edge and O K-edge XANES spectra of Ti-PA and Ti-PA-H_2O_2.

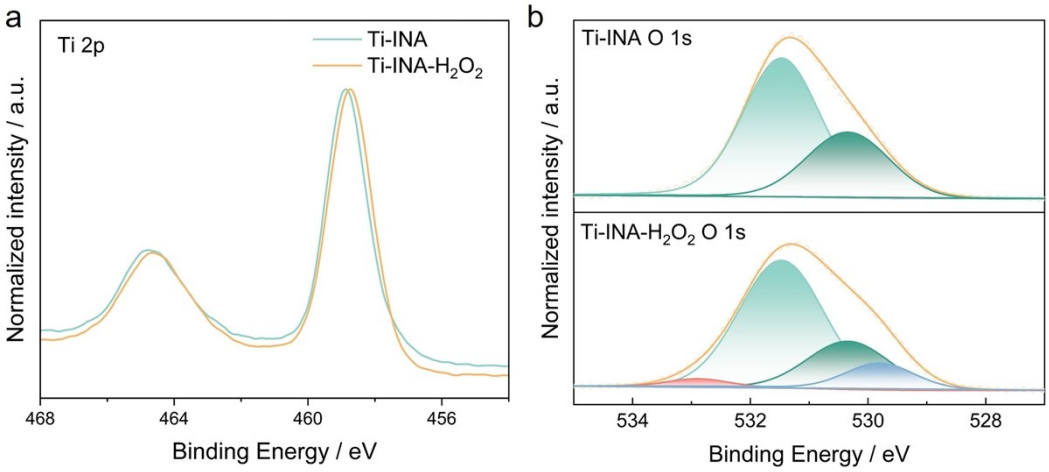

Figure S14. High-resolution (a) Ti 2p and (b) O 1s XPS spectra of Ti-INA and Ti-INA-H_2O_2.

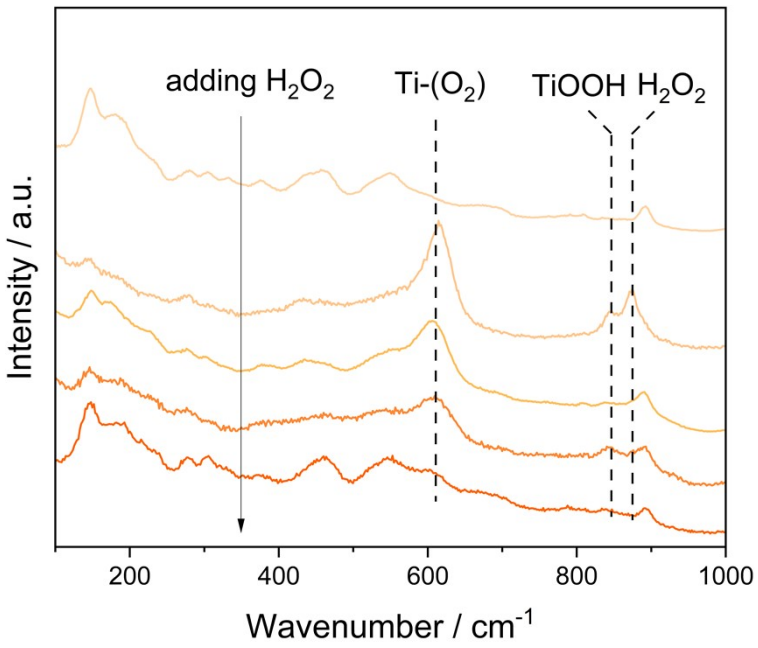

Figure S15. In-situ Raman spectra for Ti-PA when adding H_2O_2.

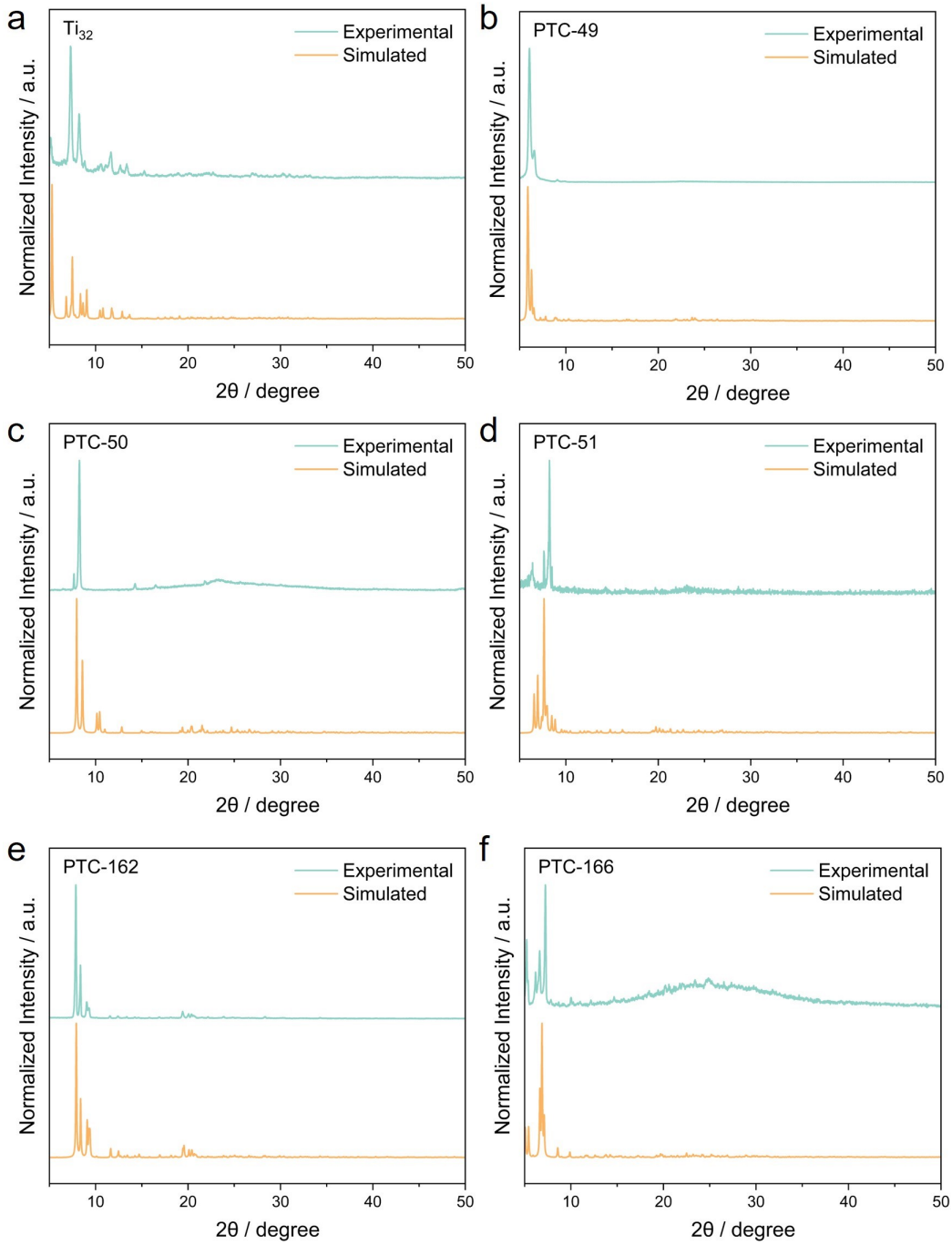

Figure S16. Experimental and simulated XRD patterns of propionic acid coordinated titanium-oxo clusters: (a) Ti_{32}: $Ti_{32}(\mu_2\text{-}O)_8(\mu_3\text{-}O)_8(OCH_2CH_2O)_{32}(PA)_{16}(OCH_2CH_2OH)_{16}$; (b) PTC-49: $Ti_{20}(\mu_2\text{-}O)_8(\mu_3\text{-}O)_{20}(PA)_{14}(8\text{-}OQ)_{10}$; (c) PTC-50: $Ti_6(\mu_3\text{-}O)_6(PA)_6(O^iPr)_6$; (d) PTC-51: $H_2[Ti_{18}(\mu_3\text{-}O)_{14}(\mu_2\text{-}O)_6(O_3P\text{-}Phen)_2(PA)_{16}(O^iPr)_{14}]$; (e) PTC-162: $Ti_6(\mu_3\text{-}O)_6(PA)_6(O^tBu)_6$; (f) PTC-166: $Ti_{44}(\mu_2\text{-}OH)_4(\mu_2\text{-}O)_{32}(\mu_3\text{-}O)_{30}(HPA)_4(PA)_{44}(GA)_2(H_2O)_2\cdot 5HPA$. PA = propionic acid; 8-OQ = 8-hydroxyquinoline; GA = glutaric acid.

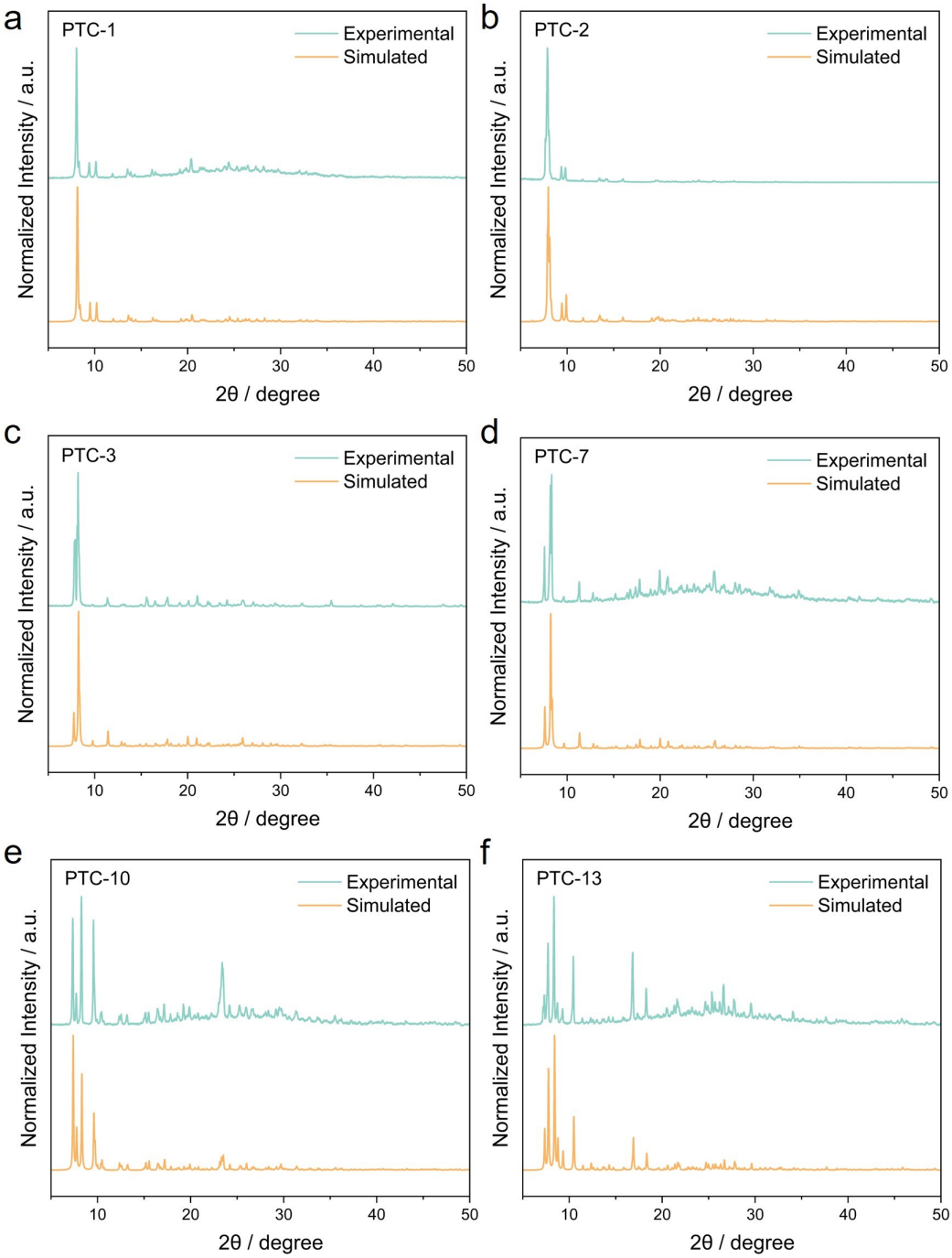

Figure S17. Experimental and simulated XRD patterns of titanium-oxo clusters of Ti_6P_2 skeleton: (a) PTC-1: $Ti_6O_4(O^iPr)_{10}(O_3P\text{-}Phen)_2(AC)_2$; (b) PTC-2: $Ti_6O_4(O^iPr)_{10}(O_3P\text{-}Phen)_2(PA)_2$; (c) Ti-INA（PTC-3）: $Ti_6O_4(O_iPr)_{10}(O_3P\text{-}Phen)_2(INA)_2$; (d) PTC-7: $Ti_6O_4(O^iPr)_{10}(O_3P\text{-}Phen)_2(BA)_2$; (e) PTC-10: $Ti_6O_4(O^iPr)_{10}(O_3P\text{-}Phen)_2(NA)_2$; (f) PTC-13: $Ti_6O_4(O^iPr)_{10}(O_3P\text{-}Phen)_2(PFBA)_2$. AC = acetic acid; PA = propionic acid; INA = isonicotinic acid; BA = benzoic acid; NA = naphthoic acid; PFBA = pentafluorobenzoic acid.

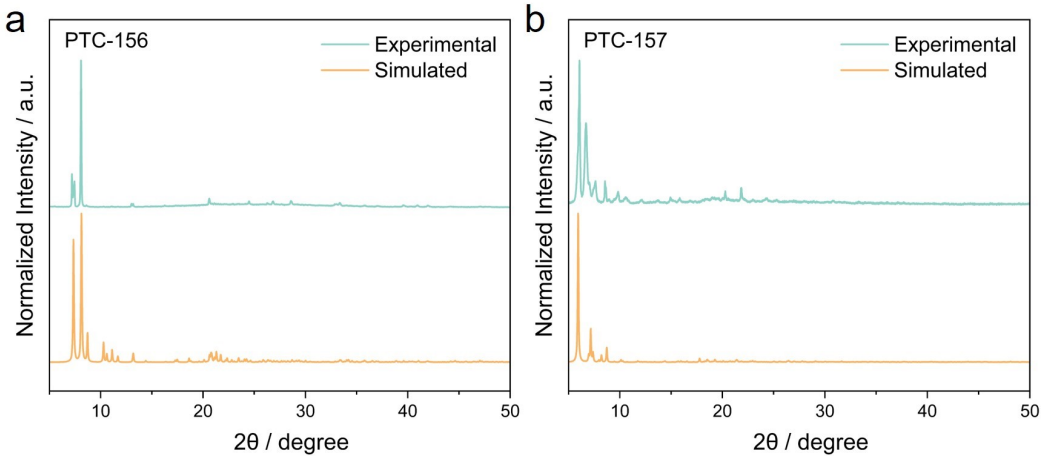

Figure S18. Experimental and simulated XRD patterns of other alkyl carboxylic acid coordinated titanium-oxo clusters: (a) PTC-156: $Ti_6(\mu_3\text{-}O)_6(^{n}PrCOO)_6(O^{i}Pr)_6$; (b) PTC-157: $Ti_{18}(\mu_2\text{-}OH)_2(\mu_2\text{-}O)_8(\mu_3\text{-}O)_{14}(^{t}BuCOO)_{14}(O^{t}Bu)_6(O^{n}Bu)_6$.

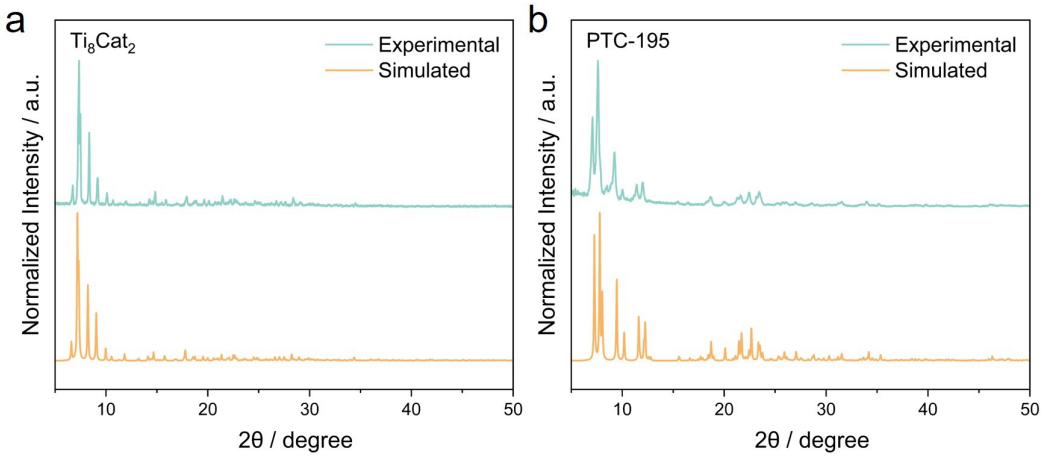

Figure S19. Experimental and simulated XRD patterns of catechol coordinated titanium-oxo clusters: (a) Ti_8Cat_2: $Ti_8(\mu_3\text{-}O)_2(\mu_2\text{-}O)_2(\mu_2\text{-}O^{i}Pr)_4(O_iPr)_8(O_3P\text{-}phen)_4(Cat)_2$; (b) PTC-195: $Ti_4(\mu_3\text{-}O)_2(Cat)_4(PZ)_4(O^{i}Pr)_4$. Cat = catechol; PZ= pyrazole.

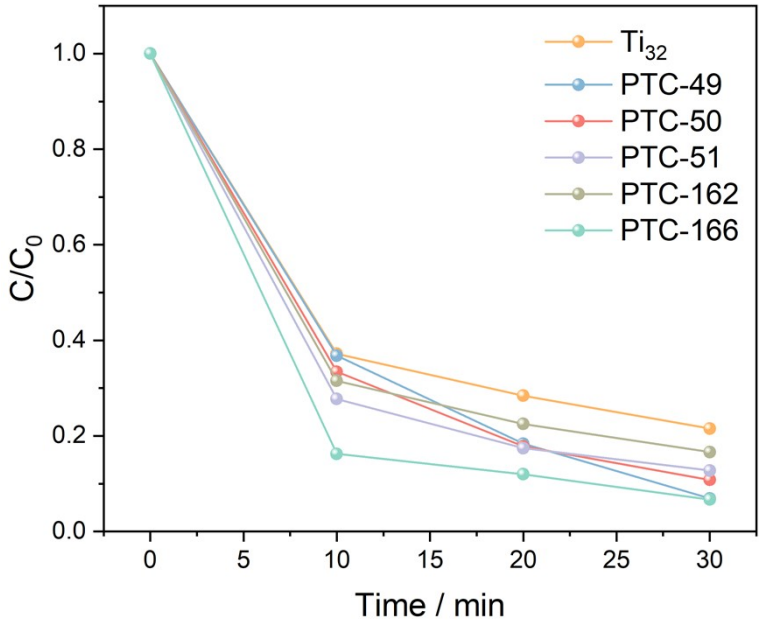

Figure S20. Fenton-like MB degradation performance of propionic acid coordinated titanium-oxo clusters[1,3,4,5].

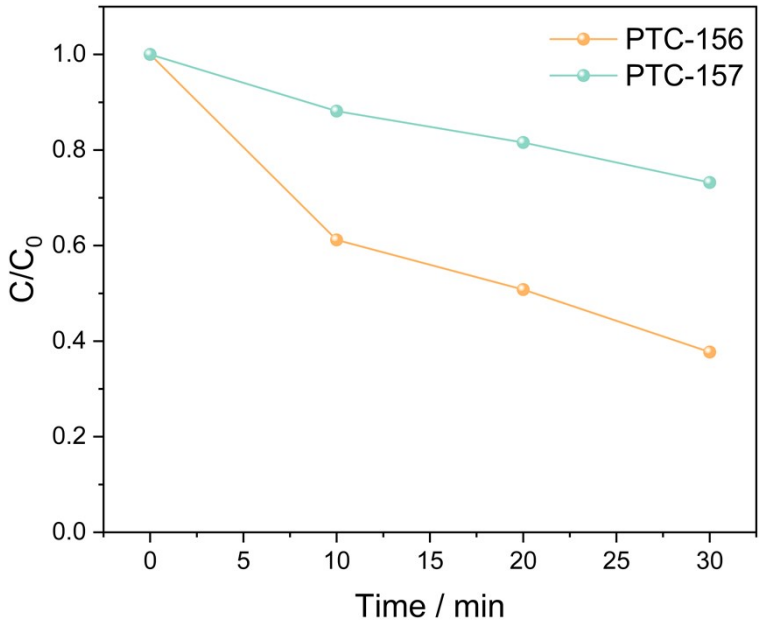

Figure S21. Fenton-like MB degradation performance of other alkyl carboxylic acid titanium-oxo clusters[1].

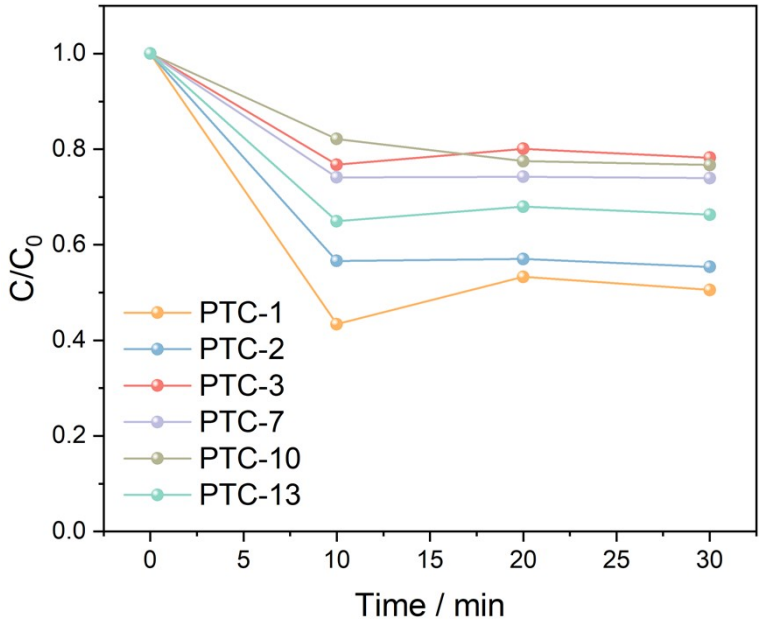

Figure S22. Fenton-like MB degradation performance of titanium-oxo clusters of Ti_6P_2 skeleton[2].

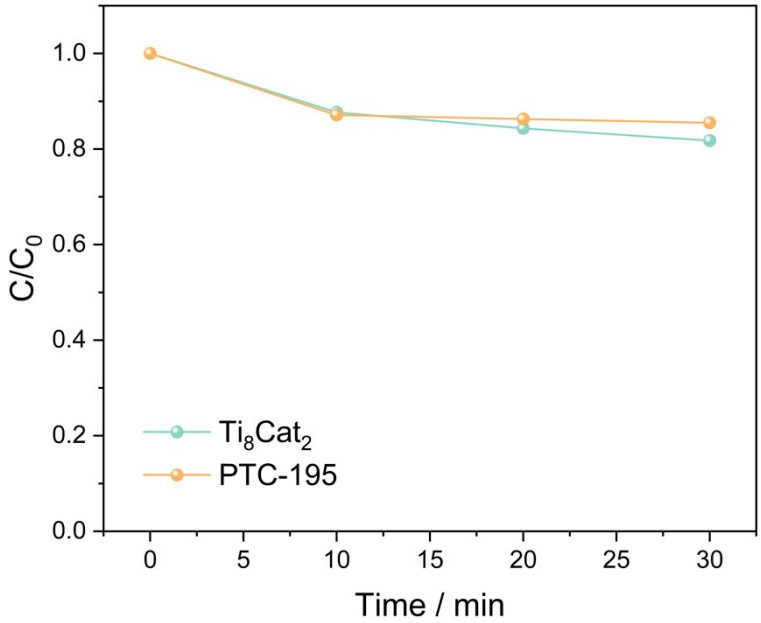

Figure S23. Fenton-like MB degradation performance of catechol coordinated titanium-oxo clusters[6,7].

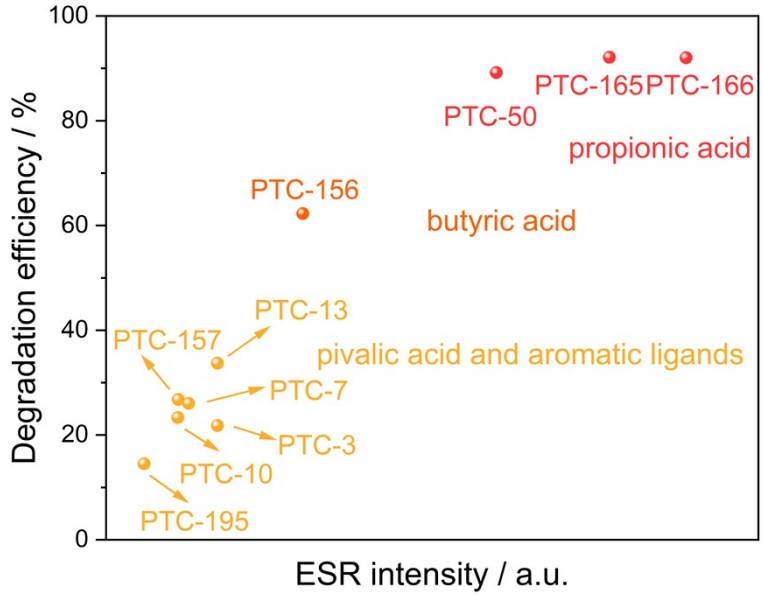

Figure S24. Comparison of MB degradation efficiency with BMPO-trapped ESR intensity.

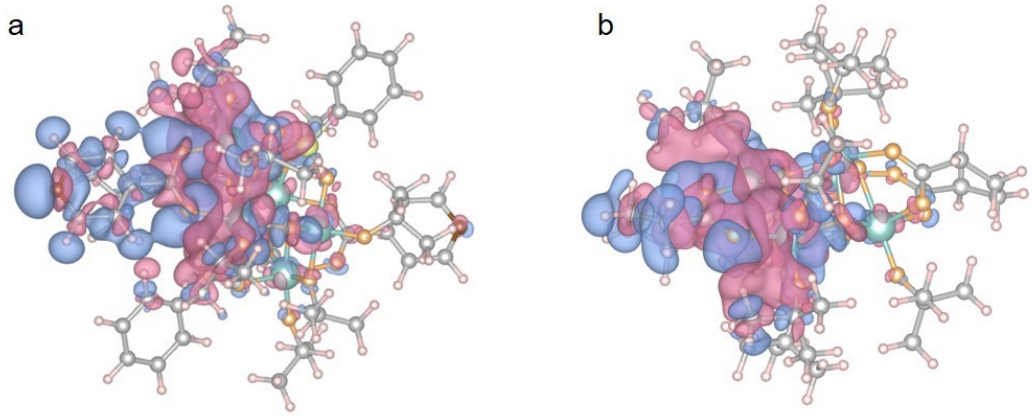

Figure S25. Differential charge density map of (a) Ti_6-INA and (b) Ti_6-PA, where red indicates electron-deficient regions and blue represents electron-rich regions.

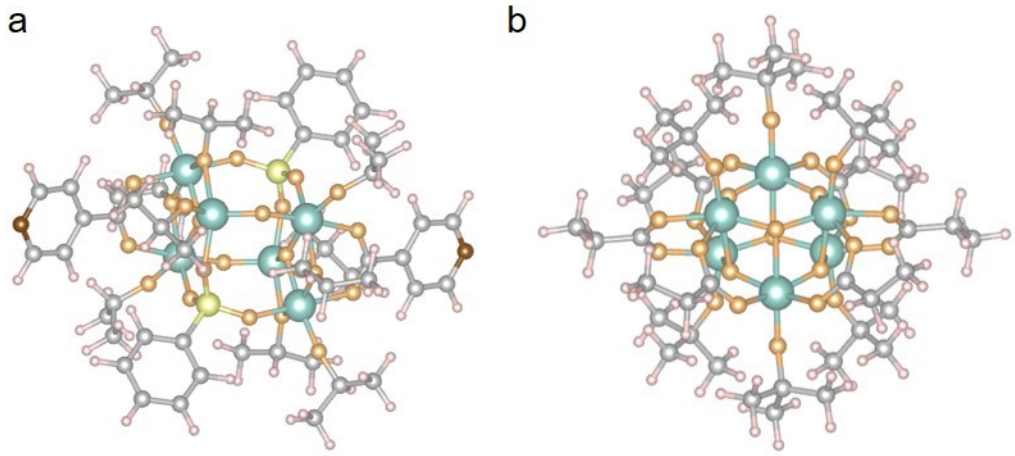

Figure S26. The structure of (a) Ti_6-INA and (b) Ti_6-PA in the step I. Atom color code: green, Ti; orange, O; grey, C; brown, N; yellow, P; pink, H.

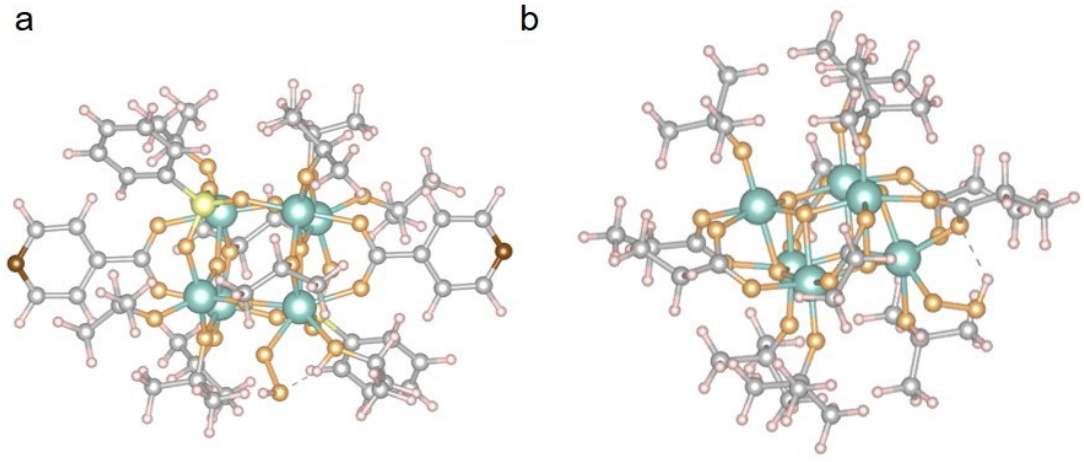

Figure S27. The structure of (a) Ti_6-INA and (b) Ti_6-PA in the step II.

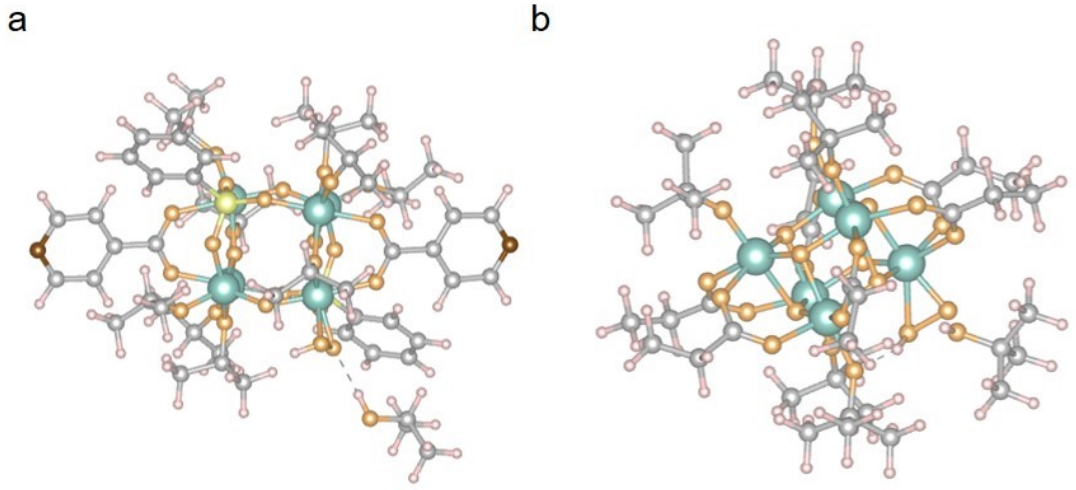

Figure S28. The structure of (a) Ti_6-INA and (b) Ti_6-PA in the step III.

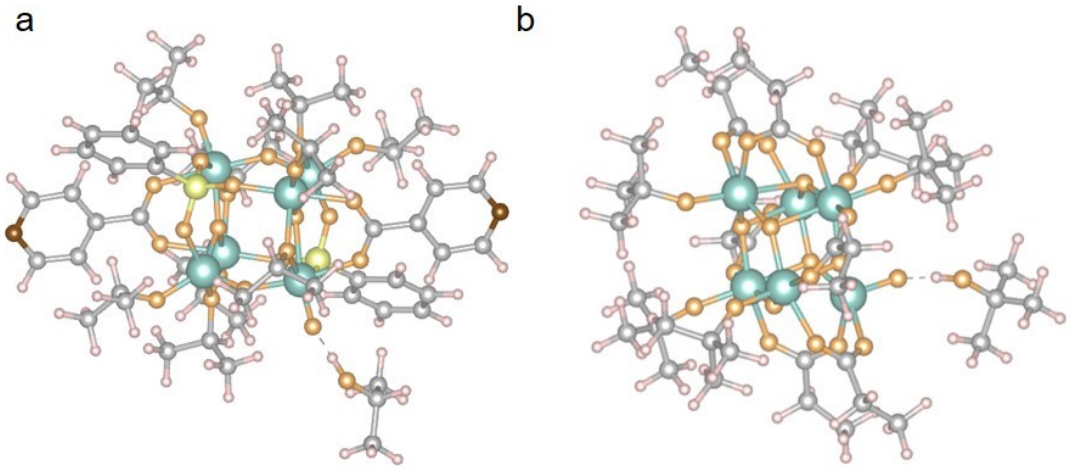

Figure S29. The structure of (a) Ti_6-INA and (b) Ti_6-PA in the step IV.

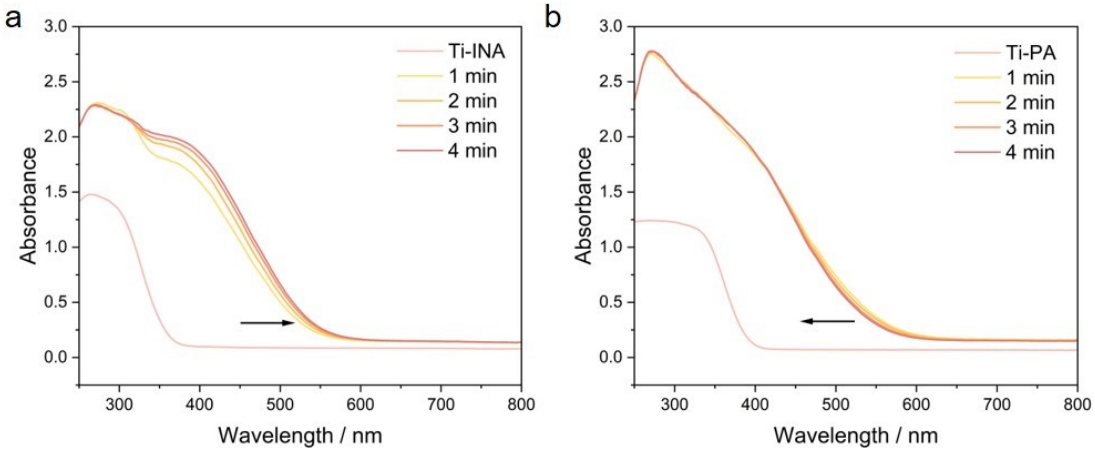

Figure S30. Time-dependent UV-vis absorption spectra of (a) Ti-INA and (b) Ti-PA upon after adding H_2O_2.

Table S1. Element contents of Ti-PA and Ti-PA-H_2O_2 from XPS measurements

Element	Ti-PA	Ti-PA-H_2O_2
C	51.78%	49.64%
Ti	9.85%	10.89%
O	38.36%	39.47%

Table S2. Bader charge of Ti_6-INA, Ti_6-PA, Ti_6-INA-OOH and Ti_6-PA-OOH

	Ti_6-INA	**Ti_6-PA**
Ti-original	1.637341	1.960862
Ti-OOH	2.248056	2.115054

References:

1. M. Y. Gao, L. Zhang and J. Zhang, *Chem. Eur. J.*, 2019, **25**, 10450-10455.
2. J. X. Liu, M. Y. Gao, W. H. Fang, L. Zhang and J. Zhang, *Angew. Chem. Int. Ed.*, 2016, **55**, 5160-5165.
3. C. Zhao, Y. Z. Han, S. Dai, X. Chen, J. Yan, W. Zhang, H. Su, S. Lin, Z. Tang, B. K. Teo and N. Zheng, *Angew. Chem. Int. Ed.*, 2017, **56**, 16252-16256.
4. X. Fan, J. Wang, K. Wu, L. Zhang and J. Zhang, *Angew. Chem. Int. Ed.*, 2018, **58**, 1320-1323.
5. W. Fang, L. Zhang and J. Zhang, *Dalton Trans.*, 2017, **46**, 803-807.
6. H. Lv, H. Li, G. Zou, Y. Cui, Y. Huang and Y. Fan, *Dalton Trans.*, 2018, **47**, 8158-8163.
7. X. Fan, H. Fu, L. Zhang and J. Zhang, *Dalton Trans.*, 2019, **48**, 8049-8052.
8. G. Kresse and J. Furthmuller, *Comput. Mater. Sci.*, 1996, **6**, 15-50.
9. P. E. Blochl, *Phys. Rev. B*, 1994, **50**, 17953-17979.
10. J. P. Perdew, J. A. Chevary, S. H. Vosko, K. A. Jackson, M. R. Pederson, D. J. Singh and C. Fiolhais, *Phys. Rev. B*, 1992, **46**, 6671-6687.
11. S. Grimme, J. Antony, S. Ehrlich and H. Krieg, *J. Chem. Phys.*, 2010, **132**, 154104.